Formation and Electronic Structures of Organoeuropium Sandwich Nanowires

ARTICLE *in* THE JOURNAL OF PHYSICAL CHEMISTRY A · APRIL 2014

Impact Factor: 2.69 · DOI: 10.1021/jp5011007 · Source: PubMed

9 AUTHORS, INCLUDING:

Ken Miyajima
The University of Tokyo
54 PUBLICATIONS **1,154** CITATIONS
SEE PROFILE

Satoshi Yabushita
Keio University
80 PUBLICATIONS **2,380** CITATIONS
SEE PROFILE

THE JOURNAL OF PHYSICAL CHEMISTRY A

Article

pubs.acs.org/JPCA

Formation and Electronic Structures of Organoeuropium Sandwich Nanowires

Natsuki Hosoya,[†] Ryuta Takegami,[†] Jun-ichi Suzumura,[†] Keizo Yada,[†] Ken Miyajima,[†] Masaaki Mitsui,[†] Mark B. Knickelbein,[‡] Satoshi Yabushita,[†] and Atsushi Nakajima*[,†,§]

[†]Department of Chemistry, Faculty of Science and Technology, Keio University, 3-14-1 Hiyoshi, Kohoku-ku, Yokohama 223-8522, Japan

[‡]Chemical Science and Engineering Division, Argonne National Laboratory, Argonne, Illinois 60439, United States

[§]JST-ERATO, Nakajima Designer Nanocluster Assembly Project, 3-2-1 Sakado, Takatsu-ku, Kawasaki 213-0012, Japan

ABSTRACT: Organoeuropium sandwich clusters, comprising europium (Eu) and 1,3,5,7-cyclooctatetraene (COT) ($Eu_n(COT)_m$), were produced in the gas phase using a laser vaporization synthesis method. Photoionization mass spectra revealed an exclusive $Eu_n(COT)_m$ formation with three compositions: $m = n + 1$, $m = n$, and $m = n - 1$, which, we propose, correspond to full-sandwich, half-sandwich, and inverted-sandwich structures, respectively. The charge distributions, metal−ligand bonding characteristics, and electronic structures of the clusters were comprehensively investigated by photoionization measurements of $Eu_n(COT)_m$ neutrals and by photoelectron spectroscopy of $Eu_n(COT)_m^-$ and isoelectronic $Ba_n(COT)_m^-$ anions. The results confirmed that (1) highly ionic metal−ligand bonding is formed between Eu^{2+} and COT^{2-} within the sandwich structure (at the termini, ionic forms are Eu^+ and COT^-) and (2) size dependence of orbital energy can be explained by the Coulombic interaction of simple point charge models between the detaching electrons and dipoles/quadrupoles. When the terminus of the sandwich clusters is Eu^{2+}, COT^{2-}, or Eu^0, the orbital energy of the electron detachment channel at the opposite terminus strongly depends on the cluster size. In this case, the molecular stack behaves as a one-dimensionally aligned dipole; otherwise, it behaves as a quadrupole, and the relationship between cluster size and electron detachment energy is much weaker. The study also reports on the 4f orbital energy in Eu ions and the formation mechanism of organoeuropium sandwich nanowires up to 12 nm in length. The nanowires are formed by successive charge transfer at the terminal part, Eu^+ and COT^-, which reduces the ionization energy and increases the electron affinity, respectively.

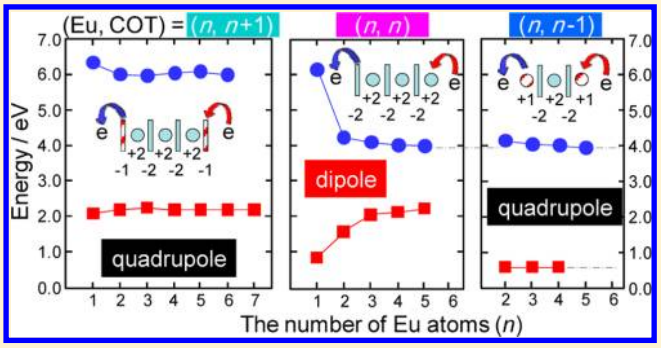

1. INTRODUCTION

Since the discovery of ferrocene [$Fe(\eta^5\text{-}C_5H_5)_2$] in 1951,[1] the coordination and synthetic chemistry of organometallic sandwich compounds has been extensively studied.[2] In particular, the first liquid-phase synthesis of triple-decker [$Ni_2(\eta^5\text{-}C_5H_5)_3$][$BF_4$] sandwich compounds[3,4] inspired the preparation of many such multiple-decker complexes.[5,6] In works that paralleled traditional liquid-phase synthetic methods, Hoshino et al. synthesized multiple-decker vanadium-benzene [$V_n(Bz)_m$] sandwich clusters (up to ∼5 layers) in the gas phase by combining laser-vaporization techniques with molecular beam methods.[7] In the past few decades, numerous experimental and theoretical studies on $V_n(Bz)_m$ clusters have unveiled their metal−ligand bonding characteristics,[8,9] geometric structures,[10,11] electronic structures,[12,14] electron spin structures,[13−22] and multilayer formation mechanism.[23]

$V_n(Bz)_m$ clusters exemplify organometallic sandwich compounds of d-block transition metal elements. The f-block actinide/lanthanide elements have also been assembled into sandwich complexes, enabling researchers to explore new functional properties resulting from 5f/4f electrons, ionic bonding characteristics, and radioactivities.[24] In 1968, a double-decker sandwich of uranocene [$U(COT)_2$] was discovered in the reaction between uranium (U) atoms and 1,3,5,7-cyclooctatetraene (COT) molecules.[25] Subsequently, many types of lanthanide (Ln)−COT sandwich compounds with Ln(COT) (Ln = Eu and Yb) and $Ln(COT)_2$ (Ln = La, Ce, Pr, Nd, Sm, Gd, and Tb) structures have been synthesized in the condensed phase.[26,27] Experimental and theoretical studies have revealed the highly ionic characteristics of the alternate metal−ligand bonding in these compounds.[26−29] Similar to $V_n(Bz)_m$ clusters, multiple-decker $Ln_n(COT)_{n+1}$ (Ln = Ce, Nd, Eu, Ho, and Yb) sandwich clusters were produced in the gas phase, and exhibited similar ionic metal−ligand bonding characteristics in experiments.[30−34] In particular, europium (Eu) and ytterbium (Yb) become divalent (+2) in these sandwich complexes

Special Issue: A. W. Castleman, Jr. Festschrift

Received: January 31, 2014
Revised: March 27, 2014

dx.doi.org/10.1021/jp5011007 | J. Phys. Chem. A XXXX, XXX, XXX−XXX

because of their half-filled $[Xe](4f)^7$ and completely filled $[Xe](4f)^{14}$ 4f-orbital configurations, respectively, whereas Ln atoms are most likely to be trivalent (+3) in compounds.[24] Previously, we reported that organoeuropium sandwiches assemble into nanowires of $Eu_n(COT)_m$ ($m = n + 1$, $m = n$, and $m = n - 1$) up to $n \sim 18$ layers.[34] The nanowire formation mechanism was found to be explained well by the so-called "harpoon" mechanism.[35] Furthermore, experiments and theoretical studies have revealed the cluster size dependence of the ionization energies (E_i's) and electron affinities (EAs) in *half-sandwich* $Eu_n(COT)_n$,[36,37] demonstrating that their electronic states are characterized by strong ionic bonding.

In this article, which includes larger half-sandwich $Eu_n(COT)_n$, we will provide a full account of experimental results on the electronic structures of three cluster compositions—*full-sandwich* $Eu_n(COT)_{n+1}$, *half-sandwich* $Eu_n(COT)_n$, and *inverted-sandwich* $Eu_n(COT)_{n-1}$ sandwich clusters—and compare them with those of isoelectronic barium (Ba)−COT clusters. Size-dependent evolution of the electronic structure is explored by photoionization and anion photoelectron spectroscopies. Employing simple point charge models,[36,37] we attribute the size dependence of orbital energy in the highly ionic metal−ligand bonding to Coulombic interactions between detaching electrons and the dipoles/quadrupoles, which are one-dimensionally stacked.

2. EXPERIMENTAL METHODS

2.1. Production and Photoionization Spectroscopy of $Eu_n(COT)_m$ Neutrals. Details of the experimental setup have been previously described.[38,39] Briefly, $Eu_n(COT)_m$ sandwich clusters were synthesized by reacting laser-vaporized Eu atoms with COT molecules. In the laser-vaporization region, the surface of a Eu rod (purity 99.9%) was vaporized by focusing a second harmonic (532 nm) pulsed Nd^{3+}:YAG laser (~30 mJ/pulse, 25 Hz). The vaporized Eu atoms were rapidly cooled by collisions in a continuous flow of helium carrier gas (purity 99.9999%, flow rate ~1000 SCCM (=std. cm^3 min^{-1})) and entrained into a temperature-controlled flow-tube reactor. In the reaction region, COT vapor diluted with helium gas (~50 SCCM) was admixed with the Eu vapor flow, such that the $Eu_n(COT)_m$ clusters were formed. After residing in the flow tube for ~4 ms (a sufficient duration to ensure that the clusters were thermally equilibrated to the flow-tube temperature (T; variable between 56 and 300 K)), the clusters were expanded into a vacuum through a 1.3 mm diameter orifice, forming a free jet which was subsequently collimated into a molecular beam.[40] Finally, the $Eu_n(COT)_m$ clusters were photoionized by an ArF excimer laser (193 nm; 6.42 eV) and detected by a time-of-flight mass spectrometer (TOF-MS).

To measure the ionization energies (E_i's) of the $Eu_n(COT)_m$ clusters, the clusters thermalized at room temperatures were ionized by a wavelength-tunable OPO (optical parametric oscillator) laser operated at photon energies ranging from 3.8 to 6.4 eV at 0.01−0.03 eV intervals. To obtain photoionization efficiency (PIE) curves, the normalized ion intensities of the mass spectra were plotted as functions of photon energy, and the E_i's of $Eu_n(COT)_m$ clusters were determined from the final decline of the PIE curves. During these measurements, the fluencies of the ArF and OPO lasers were monitored by a pyroelectric joulemeter and maintained at ~200 $\mu J/cm^2$ to avoid multiphoton ionization processes.

2.2. Photoelectron Spectroscopy of $Eu_n(COT)_m^-$ and $Ba_n(COT)_m^-$ Anions. $Eu_n(COT)_m^-$ cluster anions were also produced by the above-mentioned methods at room temperature. To record the photoelectron (PE) spectra, the cluster anions were coaxially extracted by a pulsed electric field of −3.0 kV for mass analysis or by −1.5 kV for photoelectron spectroscopy (PES) measurements. After the cluster beam was decelerated, the mass-selected cluster anions were photodetached by a third harmonic (355 nm, 3.49 eV) and a fifth harmonic (213 nm, 5.82 eV) pulsed Nd^{3+}:YAG laser. The PE signal was accumulated to 30 000−50 000 shots by a multichannel scaler/averager. The resolution at 1 eV electron energy was approximately 50 meV fwhm. The PE kinetic energy was calibrated by the $^1S_0 \rightarrow {}^2S_{1/2}$ and $^1S_0 \rightarrow {}^2D_{5/2}$ transitions of Au^-.[41,42] The photodetachment laser power ranged from 1 to 5 mJ/cm^2 and from 10 to 20 mJ/cm^2 at 213 and 355 nm, respectively. For comparison, the PE spectra of Ba−COT cluster anions were also measured using laser-vaporized Ba rods.

3. RESULTS AND DISCUSSION

3.1. Mass Distributions of $Eu_n(COT)_m$ Clusters. Figure 1 shows the photoionization mass spectra of $Eu_n(COT)_m$ clusters

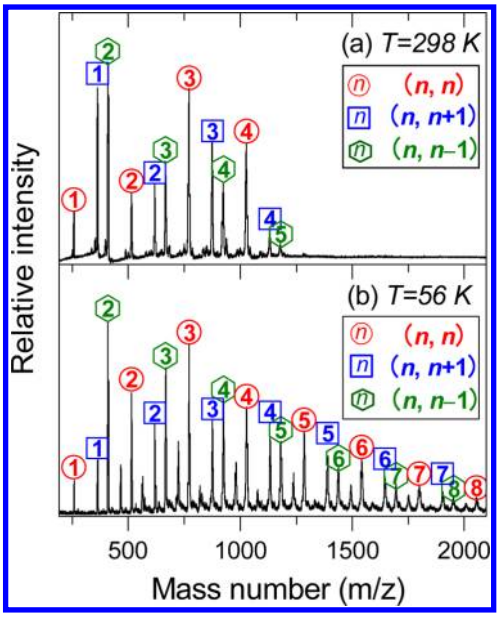

Figure 1. Time-of-flight mass spectra of neutral $Eu_n(COT)_m$ clusters measured by photoionization of an ArF excimer laser (193 nm) at (a) warm temperature (T = 298 K) and (b) cold temperature (T = 56 K). Specific compositions of full-sandwich ($m = n + 1$), half-sandwich ($m = n$), and inverted-sandwich ($m = n - 1$) clusters predominate in both spectra. Larger clusters are more abundantly formed at the cold temperature (56 K) than at 298 K.

thermalized at cluster source temperatures of (a) 298 K and (b) 56 K. In these spectra, $Eu_n(COT)_m$ is abbreviated to (n, m) for convenience, where n and m denote the number of Eu atoms and COT molecules, respectively. The mass spectra in Figure 1 reveal three abundant series of $Eu_n(COT)_m$: (n, $n + 1$), (n, n), and (n, $n - 1$). According to the previous studies of transition metal−benzene clusters,[7,12] such regular mass distribution strongly suggests that the $Eu_n(COT)_m$ clusters possess multiple-decker sandwich structures, in which Eu and COT are alternately stacked.[23,43] Hereafter, we refer to the sandwich cluster configurations as full-sandwich ($m = n + 1$), half-sandwich (one end open: $m = n$), and inverted-sandwich (both

dx.doi.org/10.1021/jp5011007 | J. Phys. Chem. A XXXX, XXX, XXX−XXX

ends open: $m = n - 1$), respectively. Although these cluster configurations predominate at 298 and 56 K, the maximum cluster size strongly depends on the cluster source temperature (T).

As evident from Figure 1, larger sandwich clusters are more abundantly formed at 56 K than at 298 K. The maximum size yielded at the cold temperature (56 K) can be greatly extended by optimizing the experimental conditions in the higher mass number regions of (a) ~3000 and (b) ~5000 amu (see Figure 2). Both spectra of Figure 2 show additional species of (n, n + 2) and (n, n + 3). Since the mass intensities of these species are largely decreased by reducing the flow rate of the COT vapor, their peaks are assigned to the full-sandwich clusters solvated by one or two additional COT molecules. Similar solvated sandwich complexes have been reported in the $V_n(Bz)_m$ cluster system at high concentrations of Bz vapor delivered at low temperature (T = 63 K).[43] Figure 2 also reveals that, with increasing cluster size, the mass intensities of the half-sandwich (n, n) clusters are enhanced relative to those of the neighboring full-sandwich (n, n + 1) and inverted-sandwich (n, n − 1) clusters. This result is attributed to the kinetic effect in the cluster growth process, i.e., the number of reaction sites in the cluster, as discussed in detail in the next section.

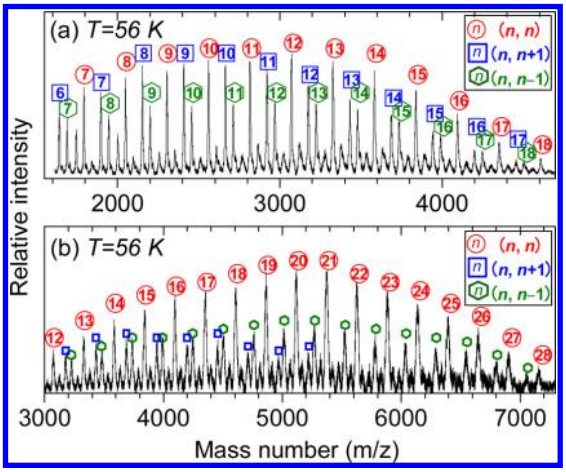

Figure 2. Time-of-flight mass spectra of neutral $Eu_n(COT)_m$ clusters obtained by photoionization of an ArF excimer laser (193 nm) at T = 56 K: (a) lower mass range and (b) higher mass range. In these spectra, three series of $Eu_n(COT)_m$ clusters are produced in multidecker sandwich configurations (up to n ~30).

3.2. Electronic Spectroscopy of $Eu_n(COT)_m$ Clusters. The charge distributions and the metal−ligand bonding characteristics of the $Eu_n(COT)_m$ clusters were investigated by photoionization measurements of neutral $Eu_n(COT)_m$ and anion PES measurements of $Eu_n(COT)_m^-$. In particular, the anion PES provides quantitative information on the relevant electronic states including the low-lying electronic excited states of neutral species.[44,45]

The electron configurations of individual Eu and COT components in ionically bonded $Eu_n(COT)_m$ clusters can be principally characterized as follows. The valence electron configurations of the ground states of Eu^{2+}, Eu^+, and Eu are described as $(4f)^7$, $(4f)^7(6s)^1$, and $(4f)^7(6s)^2$, respectively, in which the 4f electrons form a half-filled shell structure with a core-like character. On the other hand, based on their symmetries, the eight π molecular orbitals on the COT ligand (L) are denoted, based on their symmetries, as nondegenerate Lσ; doubly degenerate Lπ, Lδ, and Lϕ; and nondegenerate Lγ. Therefore, the valence electron configurations of COT, COT^-, and COT^{2-} are $(L\sigma)^2(L\pi)^4(L\delta)^2$, $(L\sigma)^2(L\pi)^4(L\delta)^3$, and $(L\sigma)^2(L\pi)^4(L\delta)^4$, respectively, where COT^{2-} satisfies the Hückel rule of 10 π electrons. From these electron configurations, we can elucidate the electronic structures. Moreover, the formal charges are easily determined by counting the number of electrons in the valence orbitals, namely, the 6s and Lδ orbitals, because each orbital is localized on Eu or COT.

Figure 3 shows the formal charge distributions of the electronic ground/excited states of anionic, neutral, and cationic species of $Eu_n(COT)_{n+1}$, $Eu_n(COT)_n$, and $Eu_n(COT)_{n-1}$ clusters. In this figure, the solid (red), striped, and open (gray) circles denote neutral, +1, and +2 charged Eu, respectively, while the solid (red), striped, and open (gray) rectangles denote neutral, −1, and −2 charged COT, respectively.

3.2.1. Ionization Energies of $Eu_n(COT)_m$ Clusters. Parts a, b, and c of Figure 4 plot the experimental photoionization efficiency (PIE) curves at different sizes of full-sandwich (n, n + 1), half-sandwich (n, n), and inverted-sandwich (n, n − 1) clusters, respectively. The E_i's were obtained from the final decline of the PIE curve. In each plot, the downward arrow indicates the E_i listed in Table 1.

Full-Sandwich Cluster. The E_i's of the full-sandwich $Eu_n(COT)_{n+1}$ (n = 1−6) are weakly dependent on cluster size. After decreasing by 0.35 eV from n = 1 to 2, the E_i remains almost constant at ~6.0 eV. In the full-sandwich clusters, the orbital contributing to the ionization process is considered to be discontinuously localized along the molecular axis, because the cluster is bound by ionic bonding and the positive/negative charge is localized at each Eu/COT component.[30] In the full-sandwich neutrals, all of the Eu atoms preferentially exist in the +2 oxidation state, while the sandwiched COT(s) is (are) doubly charged (COT^{2-}), and both ends of COT are singly charged (COT^-), as shown in Figure 3b.

This ionization channel can be understood qualitatively under the one-electron approximate description that an electron is detached from one of these ionic components; the three candidates of first ionization channels are (i) $Eu^{2+} \rightarrow Eu^{3+}$, (ii) $COT^- \rightarrow COT^0$, and (iii) $COT^{2-} \rightarrow COT^-$. However, candidate iii is promptly excluded because the COT molecules in $Eu_1(COT)_2$ are singly charged COT^- at both ends. Moreover, the COT^{2-} in larger $Eu_n(COT)_{n+1}$ clusters is highly stabilized by its two neighboring Eu^{2+} ions.[30,31] The energies of candidates i and ii have been reported to be 24.92 and 0.58 eV, respectively.[46−48] Comparing these two values, it is most likely that the ionization channel of ii, $COT^- \rightarrow COT^0$, is the lowest-energy ionization channel in the full-sandwich clusters (see Figure 3a).

Half-Sandwich Cluster. A previous study reported E_i data for $Eu_n(COT)_n$ (n = 1−4).[36] In the present study, the E_i values up to n = 5 were determined as 6.10, 4.25, 4.10, 4.01, and 3.98 eV, respectively. The half-sandwich neutrals comprise alternating $Eu^{2+}COT^{2-}$ units (state X in Figure 3e; note in the present paper the state label X is used exclusively for these closed-shell electronic states, and the state label convention has been changed from the previous work[36]). In the density functional theory (DFT) calculations,[36] these alternating $Eu^{2+}COT^{2-}$ units can be regarded as one-dimensional (1D) stacks of a dipole array (see Figure 3). The highest occupied molecular orbital (HOMO) of $Eu_n(COT)_n$, located in the terminal COT^{2-}, is successively destabilized with each additional

dx.doi.org/10.1021/jp5011007 | J. Phys. Chem. A XXXX, XXX, XXX−XXX

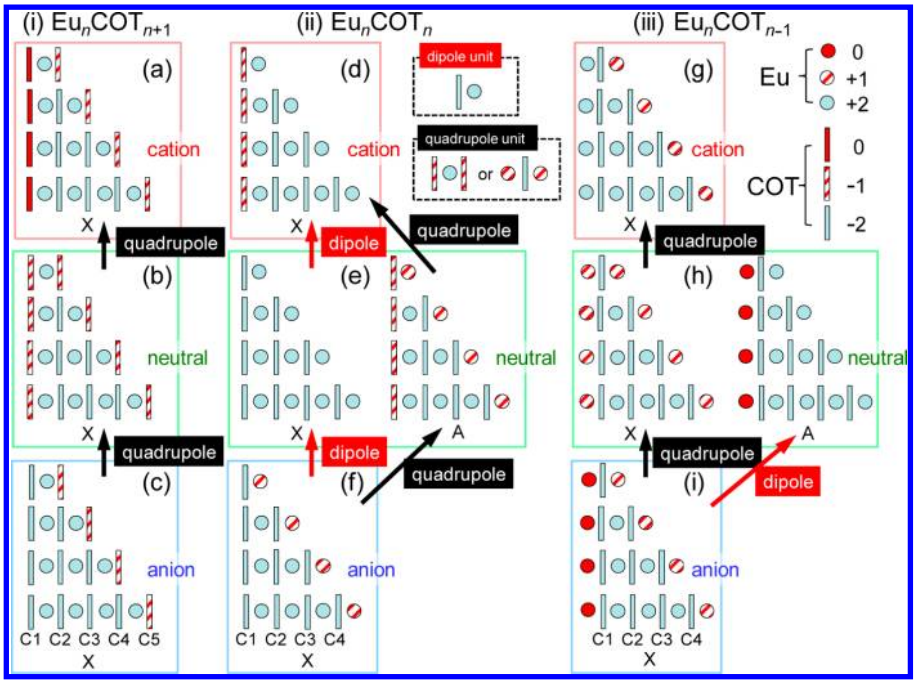

Figure 3. The formal charge distributions in the electronic ground (X) and excited (A) states of anionic, neutral, and cationic species of $Eu_n(COT)_{n+1}$, $Eu_n(COT)_n$, and $Eu_n(COT)_{n-1}$ clusters. Depending on the detachment channel, the detaching electron experiences a dipole or quadrupole effect from the remainder of the ionically charged 1D component. When one terminal of the sandwich clusters is Eu^{2+}, COT^{2-}, or Eu^0, the orbital energy of the detachment channel at the opposite terminal strongly depends on cluster size, because the 1D stack exerts a dipole effect; otherwise, it exerts a quadrupole effect and the relationship between cluster size and electron detachment energy is much weaker. Units of dipole and quadrupole are also shown in the top center. For larger (n, n) neutral, the A state becomes more stable than the X state owing to the 1D dipole stack (see text in section 3.2.2).

$Eu^{2+}COT^{2-}$ dipole unit. Therefore, the terminal COT^{2-} and the terminal Eu^{2+} of the larger half-sandwich neutral comes to be COT^- and Eu^{1+}, respectively (see state A in Figure 3e).[37] This charge distribution at the termini plays a crucial role in the subsequent reaction of the full-sandwich formation because it lowers the E_i of $Eu_n(COT)_n$.

Inverted-Sandwich Cluster. The E_i's of the inverted-sandwich $Eu_n(COT)_{n-1}$ clusters are ~4 eV for n = 2−5. Thus, the E_i's of $Eu_n(COT)_{n-1}$ demonstrate similar size independence to those of full-sandwich $Eu_n(COT)_{n+1}$ but are approximately 2 eV smaller. All of the COT molecules in the inverted-sandwich neutrals adopt the −2 oxidation state, while the sandwiched and terminal Eu atoms adopt +2 and +1 oxidation states, respectively. Analogous to the full-sandwich $Eu_n(COT)_{n+1}$, candidates of the first ionization channel of inverted-sandwich $Eu_n(COT)_{n-1}$ are (i) $Eu^+ \rightarrow Eu^{2+}$, (ii) $Eu^{2+} \rightarrow Eu^{3+}$, and (iii) $COT^{2-} \rightarrow COT^-$. However, candidate ii is immediately excluded because the Eu atoms in $Eu_2(COT)_1$ exist as Eu^+, and the E_i of candidate ii (24.92 eV) is much higher than that of candidate i (11.24 eV).[48] Candidate iii is also excluded because the E_i of the $Na_2(COT)_1$ complex is 5.6 eV; thus, the E_i of candidate iii far exceeds 4 eV. Here the ionization is contributed by the COT^{2-} moiety sandwiched between two Na^+ ions. Hence, the first ionization of the inverted-sandwich $Eu_n(COT)_{n-1}$ may be considered to occur at the terminal Eu^+ site via candidate (i) $Eu^+ \rightarrow Eu^{2+}$ (Figure 3g).

3.2.2. Electron Affinities of $Eu_n(COT)_m$ Clusters. In the previous subsection, the E_i's and their first ionization sites were determined for $(n, n+1)$, (n, n), and $(n, n-1)$ neutrals. This subsection evaluates the electron affinities (EAs) and the electron acceptor sites of the $Eu_n(COT)_m$ clusters. In the PE spectra shown in Figures 5 and 6, the horizontal axis indicates the electron binding energy E_b, defined as $E_b = h\nu - E_k$, where E_k is the PE kinetic energy and $h\nu$ is the photon energy of the detachment laser. The threshold of the first peak corresponds to the adiabatic detachment energy (ADE) which is often approximated as the (adiabatic) EA of the $Eu_n(COT)_m$ clusters. The vertical detachment energy (VDE) can also be derived from the peak maxima in the PE spectra.

Full-Sandwich Cluster. Parts a and b of Figure 5 show the PE spectra of full-sandwich $Eu_n(COT)_{n+1}^-$ and $Ba_n(COT)_{n+1}^-$ anions (n = 1−7), respectively, measured by the 355 and 213 nm photodetachment laser. In all of the 355 nm PE spectra, the first peak (corresponding to the VDE) appears at ~2.6 eV, with a threshold (corresponding to the ADE) of ~2.2 eV. In the full-sandwich $Eu_n(COT)_{n+1}^-$ anions, an extra electron is accommodated at the terminal end of COT^{2-}, as shown in Figure 3c. Therefore, the lowest electron detachment energy from terminal COT^{2-} imposes a relatively high EA of ~2.2 eV. A previous study reported that the number of peaks in the PES increases with increasing size of the $Eu_n(COT)_n^-$ (n = 1−4) clusters.[37] In Figure 5a (or 5b), these peaks are labeled as C1−C4, attributable to electron detachment from COT molecules in Figure 3c. In the following section, we discuss how the peaks are related to the electron detachment from the COTs.

Half-Sandwich Cluster. We have extended our PES measurements, previously reported for n = 1−4,[37] to include n = 5. Parts a and b of Figure 6 show the PE spectra of half-sandwich $Eu_n(COT)_n^-$ and $Ba_n(COT)_n^-$ anions (n = 1−5) at 355 and 213 nm. Two peaks, labeled M and C1, appear in the 355 nm PE spectra of n = 1 and 2. The M and C1 peaks have been previously assigned to photodetachment of the terminal $Eu^+ \rightarrow Eu^{2+}$ and the terminal $COT^{2-} \rightarrow COT^-$, respectively.[37] It is noted that the positions of the two peaks represent the

dx.doi.org/10.1021/jp5011007 | J. Phys. Chem. A XXXX, XXX, XXX−XXX

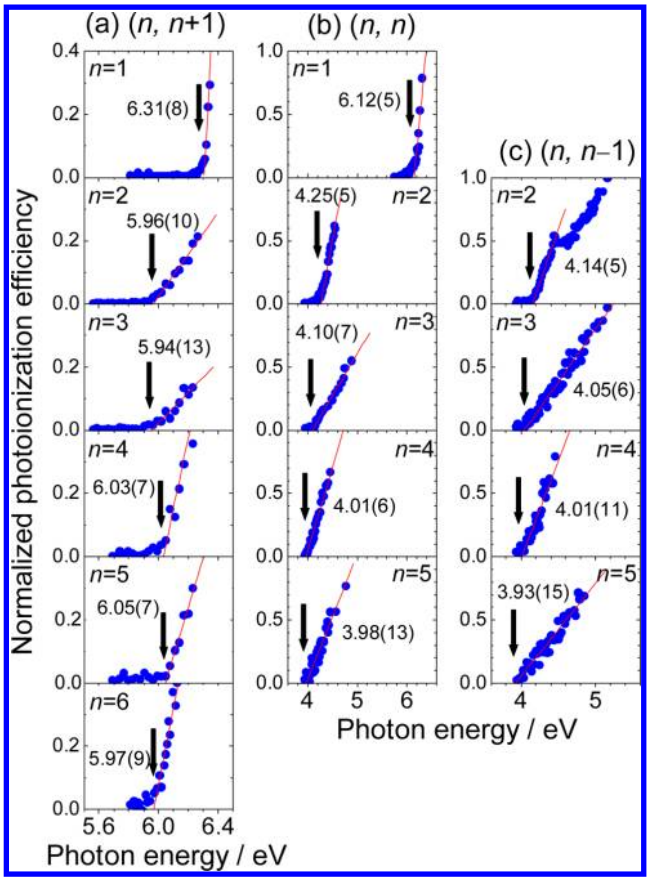

Figure 4. Typical PIE curves for $Eu_n(COT)_m$ clusters of (a) $m = n + 1$, (b) $m = n$, and (c) $m = n - 1$. The ionization energies (E_i's) are determined from the final decline of the curve: the ionization threshold is indicated by the downward arrow. The E_i's of $m = n + 1$ and $m = n - 1$ are approximately 6.0 and 4.0 eV, respectively, regardless of cluster size. In contrast, the E_i's of $m = n$ are clearly dependent on cluster size, decreasing drastically from $n = 1$ to $n = 2$ and asymptotically decreasing from $n = 2$ to $n = 5$.

relative stability of the two electronic structures X and A of the $Eu_n(COT)_n$ neutral shown in Figure 3e. As the cluster size increases, the M peak markedly shifts toward the higher energy side; i.e., the VDE increases from 1.2 eV ($n = 1$) to 1.9 eV ($n = 2$), 2.4 eV ($n = 3$), and 2.7 eV ($n = 4$). In contrast, the VDE of the C1 peak remains almost constant around 2.7 eV. For $n = 3$ and 4, the spectral profile is reasonably fitted to a pair of Gaussian functions around the M and C1 peaks, with both peaks completely overlapping at $n = 4$. Although the spectral profile at $n = 5$ is not easily fitted in this way, the M and C1 peaks must also overlap (or merge) at this size. As mentioned above, the half-sandwich $Eu_n(COT)_n^-$ anions accommodate an extra electron at their Eu termini (reducing them to Eu^+). This localized electron is stabilized with increasing cluster size by the additional $Eu^{2+}COT^{2-}$ dipole units; electron detachment from terminal Eu^+ takes place for smaller $n = 1$ and 2 clusters. However, as the cluster enlarges ($n > 3$) and the electron stabilizes, its detachment energy increases to that of electron detachment from the opposite side of COT^{2-}, yielding a relatively high EA (~2.2 eV).

For $Eu_n(COT)_n$ neutrals (Figure 3e), as the size n increases, the A state (diradical states) with these two open-shell orbitals becomes more stable than the X state (closed-shell singlet states) because the electric field by the 1D dipole stack

Table 1. Ionization Energies (E_i's) and Electron Affinities (EAs) of Multiple-Decker $Eu_n(COT)_m$ Sandwich Clusters in eV[a]

composition (n, m)	E_i	EA
	(a) Full-Sandwich	
(1, 2)	6.31 (8)	2.10 (7)
(2, 3)	5.96 (10)	2.22 (8)
(3, 4)	5.94 (13)	2.25 (10)
(4, 5)	6.03 (7)	2.22 (6)
(5, 6)	6.05 (7)	2.21 (6)
(6, 7)	5.97 (9)	2.20 (11)
(7, 8)		2.21 (12)
	(b) Half-Sandwich	
(1, 1)	6.12 (5)	0.88 (8)
(2, 2)	4.25 (5)	1.61 (9)
(3, 3)	4.10 (7)	2.09 (8)
(4, 4)	4.01 (6)	2.17 (18)
(5, 5)	3.98 (13)	2.26 (10)
	(c) Inverted-Sandwich	
(2, 1)	4.14 (5)	0.59 (4)
(3, 2)	4.05 (6)	0.60 (4)
(4, 3)	4.01 (11)	0.60 (4)
(5, 4)	3.93 (15)	

[a]Numbers in parentheses indicate experimental uncertainties; e.g., 6.31 (8) represents 6.31 ± 0.08 eV.

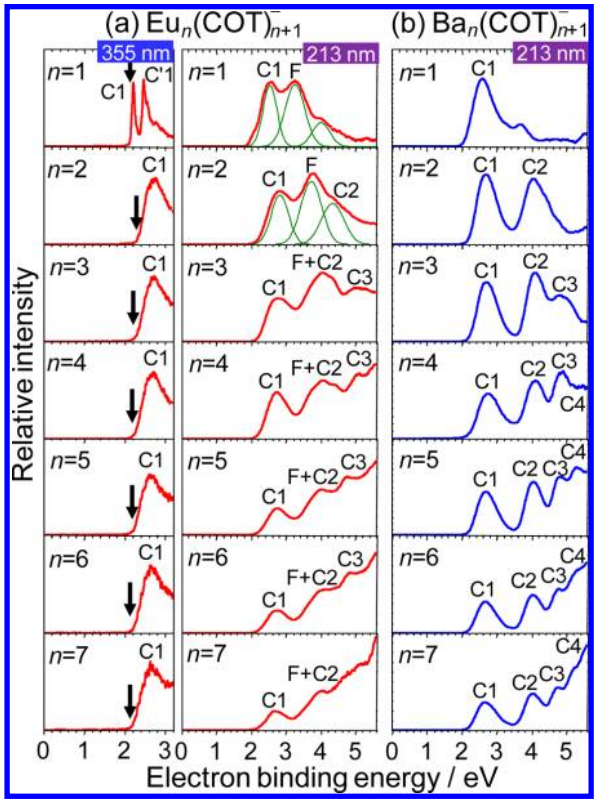

Figure 5. PE spectra of full-sandwich anions of (a) $Eu_n(COT)_{n+1}^-$ at 355/213 nm and (b) $Ba_n(COT)_{n+1}^-$ at 213 nm. The downward arrow in the 355 nm spectra indicates the adiabatic EA of the cluster.

influences the frontier orbitals; in the X state, Lδ on C1 is destabilized, while the empty 6s orbital on the opposite terminal Eu^{2+} is stabilized.[36] The switchover size has been calculated to be between $n = 2$ and $n = 3$ in our previous DFT study,[36] and it is experimentally between $n = 3$ and $n = 4$, as

dx.doi.org/10.1021/jp5011007 | J. Phys. Chem. A XXXX, XXX, XXX−XXX

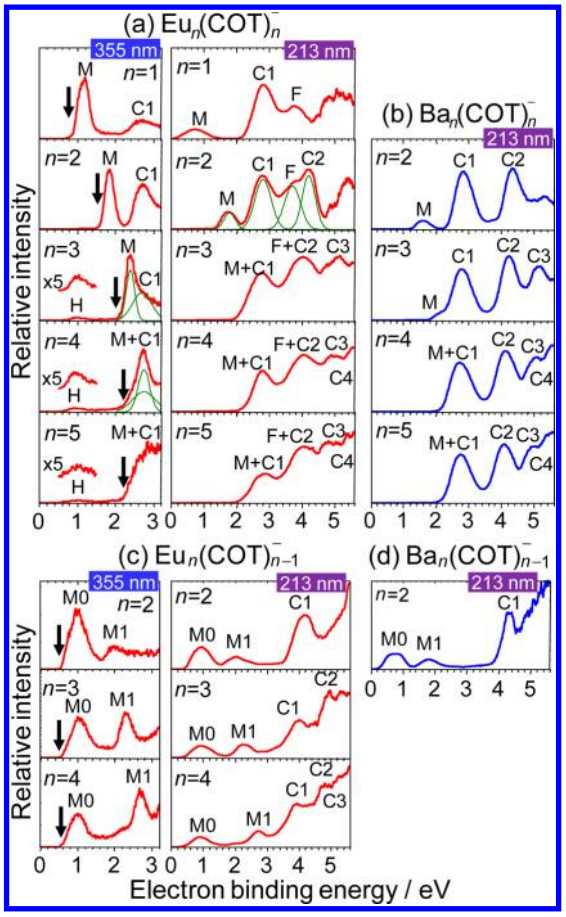

Figure 6. PE spectra of half-sandwich anions of (a) $Eu_n(COT)_n^-$ at 355/213 nm and (b) $Ba_n(COT)_n^-$ at 213 nm and those of inverted-sandwich anions of (c) $Eu_n(COT)_{n-1}^-$ at 355/213 nm and (d) $Ba_n(COT)_{n-1}^-$ at 213 nm. The downward arrow in the 355 nm spectra indicates the adiabatic EA of the cluster. Two peaks in the 355 nm spectrum of $Eu_3(COT)_3^-$ and $Eu_4(COT)_4^-$ are deconvoluted into Gaussian profiles, although the $Eu_5(COT)_5^-$ anion spectrum is not properly fitted by this model.

shown in Figure 6a, although the two states seem almost degenerate at n = 3 and 4.

Inverted-Sandwich Cluster. Figure 6c shows the PE spectra of the inverted-sandwich $Eu_n(COT)_{n-1}^-$ anions (n = 2−4) at 355 and 213 nm. For comparison, the PE spectrum of $Ba_2(COT)_1^-$ at 213 nm is shown in Figure 6d. The PE spectra of larger $Ba_n(COT)_{n-1}^-$ anions are not shown, since their peaks were obscured by low ion intensities. The PE spectrum at 355 nm shows two significant peaks, labeled M0 and M1. In the neutral $Eu_n(COT)_{n-1}$ clusters, we argued that all COT molecules exist in the −2 state; thus, the excess electron for the corresponding anion must attach to either of the terminal Eu^+ ions, producing a terminal Eu^0 atom, as illustrated in Figure 3i.

3.2.3. Cluster Size Dependence of E_i and EA. The relationships between the E_i or EA and the cluster size of $Eu_n(COT)_{n+1}$, $Eu_n(COT)_n$, and $Eu_n(COT)_{n-1}$ are plotted in Figure 7. The E_i and EA of half-sandwich $Eu_n(COT)_n$ are clearly dependent on the cluster size; however, the dependence is weakened in $Eu_n(COT)_{n+1}$ and $Eu_n(COT)_{n-1}$. These contrasting results of size-dependent photoionization and photodetachment properties can be explained by the relationship between the cluster size and the electrostatic potential experienced by the detaching electron, i.e., the Coulombic interaction between the detaching electron and the dipoles/quadrupoles.

As previously discussed,[36,37] the E_i and EA of $Eu_n(COT)_n$ (Figure 7b) arise through the detachment channel of terminal $COT^{2-} \rightarrow COT^-$ and terminal $Eu^+ \rightarrow Eu^{2+}$, respectively. As schematically shown in Figure 3e, as viewed from the terminal COT^{2-} of $Eu_n(COT)_n$ neutrals, incrementing the cluster size attaches a pair of −2 and +2 point charges to the opposite side of the cluster. This pair is regarded as an electric dipole, destabilizing the detaching electron in the COT^{2-} of $Eu_n(COT)_n$.

On the other hand, viewing from the terminal Eu^+ of $Eu_n(COT)_n^-$ anions (Figure 3f), incrementing the cluster size attaches a reversed pair of +2 and −2 point charges to the opposite side of the cluster. This electric dipole stabilizes the detaching electron in the Eu^+ of $Eu_n(COT)_n^-$. Since both destabilization and stabilization energies are inversely proportional to the square of the distance between the detaching electron and the attached dipole, the sum of destabilization/stabilization energies converges to an asymptote with increasing n, as shown in Figure 7b.

Similar point charge models can explain the cluster size independence of E_i and EA for $Eu_n(COT)_{n+1}$ and $Eu_n(COT)_{n-1}$. The E_i and EA of $Eu_n(COT)_{n+1}$ (Figure 7a)

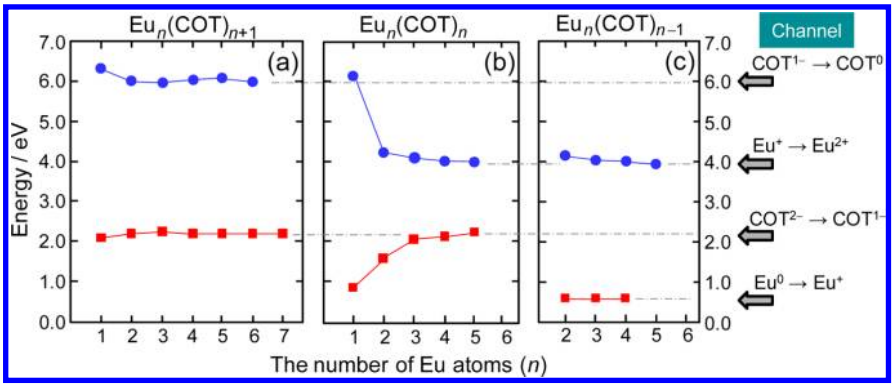

Figure 7. Cluster size dependence of E_i and EA for (a) $Eu_n(COT)_{n+1}$, (b) $Eu_n(COT)_n$, and (c) $Eu_n(COT)_{n-1}$. The electron detachment channels in the quadrupole description are shown on the right. The E_i and EA of half-sandwich $Eu_n(COT)_n$ clearly depend on cluster size, whereas the relationship is much weaker in $Eu_n(COT)_{n+1}$ and $Eu_n(COT)_{n-1}$. Note that the energies of each detachment channel are largely shifted by local Coulombic interaction with adjacent Eu^{2+} or COT^{2-} (see also Figure 3).

dx.doi.org/10.1021/jp5011007 | J. Phys. Chem. A XXXX, XXX, XXX−XXX

arise through the electron detachment channels of terminal $COT^{-} \rightarrow COT^{0}$ and terminal $COT^{2-} \rightarrow COT^{-}$, respectively. Both channels are always assigned to the electron detachment from Lδ (left terminal COT; C1) orbitals. Let us consider the relationship between cluster size and the electrostatic potential, viewed from the left-end COT in the ground state (see Figure 3a−c). In both cases, incrementing the cluster size changes the right-end COT^{-} into COT^{2-} and adds a $Eu^{2+}-COT^{-}$ pair; equivalently, a group of −1, +2, and −1 point charges are added at the right-hand side of the cluster. Since this group constitutes an electric quadruple, the stabilization energy is inversely proportional to the third power of the distance between the detaching electron on COT and the quadruple. Consequently, the electrostatic potential at the left-end COT in the ground state is almost independent of cluster size, as shown in Figure 7a.

A similar analysis can explain the E_i and EA trends of the inverted-sandwich $Eu_n(COT)_{n-1}$ clusters (see Figure 7c). The E_i and EA of $Eu_n(COT)_{n-1}$ arise through the electron detachment channels of terminal $Eu^{+} \rightarrow Eu^{2+}$ and terminal $Eu^{0} \rightarrow Eu^{+}$, respectively. Both channels are always assigned to the electron detachment from Eu(6s). Viewing from the terminal Eu^{+} or Eu^{0}, increasing the cluster size changes the right-end Eu^{+} into Eu^{2+} and adds a pair of COT^{2-} and Eu^{+}; equivalently, a group of +1, −2, and +1 point charges, behaving as a quadruple, is added to the right-hand side of the cluster (see Figure 3g−i).

We now question why Eu_nCOT_n behaves as a dipole, while Eu_nCOT_{n+1} and Eu_nCOT_{n-1} behave as a quadrupole. These behaviors are attributed to the specific natures of the detachment electron channel. Since Eu and COT preferentially adopt +2 and −2 oxidation states, respectively, the charge is completely balanced in half-sandwich Eu_nCOT_n neutrals. However, Eu_nCOT_{n+1} neutrals are deficient in two electrons, while Eu_nCOT_{n-1} neutrals contain a two-electron surplus. Thus, the charge balance in both of these clusters is upset. When removing (attaching) an electron from (to) neutrals, the same channel is used in the Eu_nCOT_{n+1} and Eu_nCOT_{n-1} neutrals; however, this channel alternates between Eu and COT in the Eu_nCOT_n neutrals. Furthermore, since charge is symmetrically distributed in practice in the Eu_nCOT_{n+1} and Eu_nCOT_{n-1} clusters, the collective ionic charge exerts a quadrupole effect on the detaching electron.

3.2.4. Electronic Structures of $Eu_n(COT)_m$ Clusters. In the preceding subsection, the electron detachment threshold energies E_i and EA, producing ground state cations and neutrals, respectively, were found to depend on cluster size. This relationship was modeled by the Coulombic interaction between the departing electron and an idealized core composed of point dipoles/quadrupoles. Moreover, several peaks in the PE spectra appear at higher electron binding energies, corresponding to electronically excited states of the corresponding neutrals. These peaks were assigned by comparing the PE spectra of $Eu_n(COT)_m^{-}$ and $Ba_n(COT)_m^{-}$ anions at 213 nm. Similar to Eu atoms, Ba atoms preferentially exist in the +2 oxidation state but possess *no* 4f electrons. Consequently, the PE spectra of $Ba_n(COT)_m^{-}$ should exhibit simpler electronic structures, uncomplicated by 4f contributions.

As shown in Figure 5b and Figure 6b, the number of spectral peaks increases with *n*. Each peak in the $Ba_2(COT)_2^{-}$ anion is assignable, as previously identified by DFT calculations for $Eu_2(COT)_2^{-}$; the first and second peaks (M and C1) are assigned to electron detachment from the terminal Ba^{+} and the opposite terminal COT^{2-}, respectively, and the third peak (C2) derives from internal COT^{2-}.[37] The VDE difference between peaks C1 and C2 can be explained by the increased stability of the central COT^{2-} relative to the terminal COT^{2-}, introduced by addition of a $Ba^{2+}COT^{2-}$ dipole unit from the left-hand side. From these assignments, we can identify each peak in the $Eu_n(COT)_m^{-}$ and $Ba_n(COT)_m^{-}$ spectra, as shown in Figures 5 and 6. For example, peaks C1 and C2 in the $Ba_2(COT)_3^{-}$ spectrum correspond to electron detachment from the terminal COT^{2-} and penultimate COT^{2-}, respectively (see Figure 3c). In this case, no detachment channel exists from the Ba atom because it retains a stable divalent state (Ba^{2+}) in full-sandwich clusters. Moreover, central COT^{2-} is also stabilized by a dipole unit, similarly to that in a half-sandwich $Ba_2(COT)_2^{-}$ cluster. Therefore, the PE spectra differ between $Ba_2(COT)_2^{-}$ and $Ba_2(COT)_3^{-}$ only by the presence or absence of peak M, resulting from the localized 6s electron in the terminal Ba^{+} ion.

Furthermore, peak M appears at a relatively low binding energy of ∼2 eV, although the *second* ionization energy of Ba atom exceeds 10 eV. This large energy difference may arise from the strong polarization of the terminal Ba^{+} ion within the half-sandwich $Ba_2(COT)_2^{-}$ anion. In fact, in our previous DFT calculations for $Eu_2(COT)_2^{-}$, the molecular orbital of the 6s electron was found to largely protrude from the nuclear center position to the outer side.[37] In the point charge model, such polarized Ba^{+} in $Ba_2(COT)_2^{-}$ corresponds to the unified $Ba^{2+}COT^{-}$ terminal within $Ba_2(COT)_3^{-}$; consequently, the energy positions of C1 and C2 are almost identical in $Ba_2(COT)_2^{-}$ and $Ba_2(COT)_3^{-}$.

On the other hand, the M0 and M1 peaks in the $Ba_2(COT)_1^{-}$ spectrum (Figure 6d) correspond to electron detachment from terminal Ba and Ba^{+}, respectively, while peak C1 derives from central COT^{2-}. Notably, the M1 and C1 peaks in the $Ba_2(COT)_1^{-}$ spectrum almost coincide with the M and C2 peaks, respectively, in the $Ba_2(COT)_2^{-}$spectrum. Considering the highly ionic bonding nature of the clusters, this suggests that the terminal Ba^{0} atom in $Ba_2(COT)_1^{-}$ is strongly polarized to the same extent as the $Ba^{2+}COT^{2-}$ dipole unit. Indeed, the VDE of peak M0 is much smaller than the first ionization energy of Ba atoms (5.21 eV),[48] verifying that the terminal Ba atom is destabilized by an electronic polarization effect.

Applying these attributes to the PE spectra of $Ba_n(COT)_m^{-}$ clusters, the peak that shifts with increasing *n* is assignable to increased numbers of COT at the right-hand side of the stack (Figure 3), because the orbital energy decreases in the left to right direction as the structure stabilizes with additional dipole $COT^{2-}Eu^{2+}$ stacking. Namely, when a COT is added to the right-hand side in Figure 3, the corresponding peak C*n* appears in the PE spectra in the order of C1−C4.

The spectra of $Eu_n(COT)_{n+1}^{-}$ and $Eu_n(COT)_n^{-}$ show a contribution at 3.3−3.8 eV (labeled "F" in Figures 5a and 6a) that is absent in the corresponding $Ba_n(COT)_{n+1}^{-}$ and $Ba_n(COT)_n^{-}$ spectra. This feature is most likely ascribed to photodetachment from the 4f orbitals of Eu.[37] Although the PE spectrum of $Ba_1(COT)_1^{-}$ could not be measured, photodetachment from the 4f orbitals of Eu in $Eu_1(COT)_1^{-}$ is presumed from comparisons of the PE spectra of $Eu_2(COT)_2^{-}$ and $Eu_3(COT)_3^{-}$. In full- and half-sandwiches, the F peak appears at almost constant energy but appears to be absent in the inverted-sandwich. From the discussion on 1D dipoles/quadrupoles, we can infer that, since an electron escaping the 4f shell experiences an electric dipole from the collective

dx.doi.org/10.1021/jp5011007 | J. Phys. Chem. A XXXX, XXX, XXX−XXX

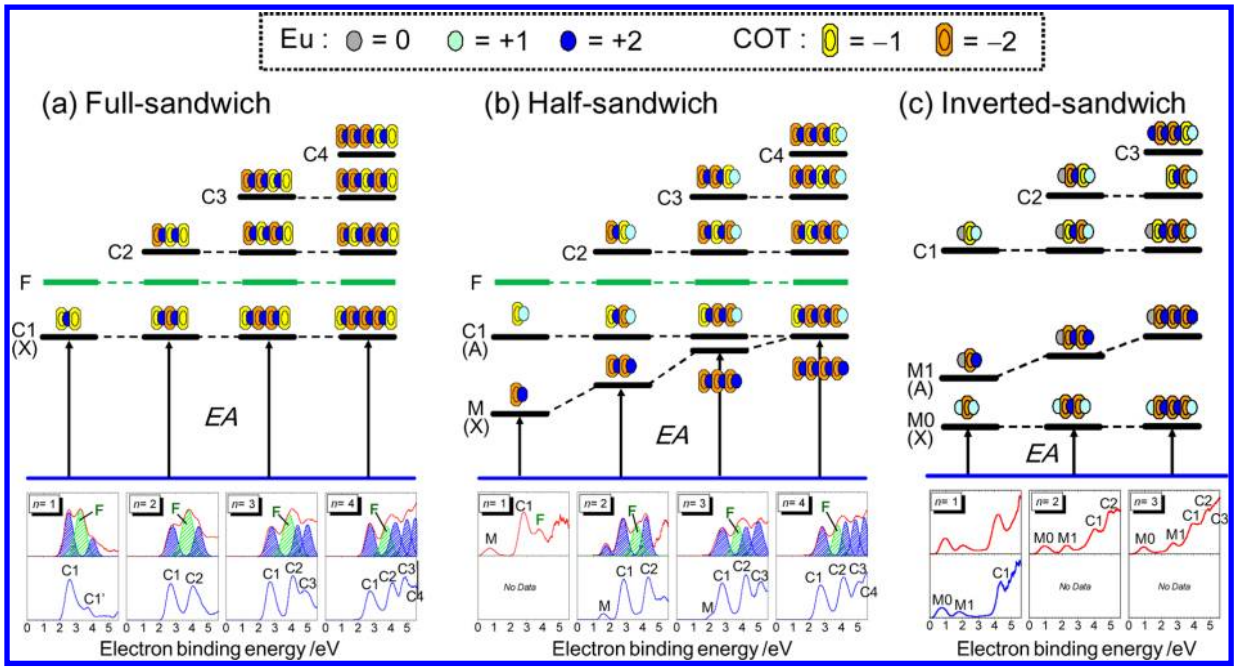

Figure 8. Energy diagram of neutral $Eu_n(COT)_m$ clusters for (a) $m = n+1$, (b) $m = n$, and (c) $m = n-1$, obtained by anion PES.

ionically charged component, 4f electron detachment should yield a second peak at a higher binding energy. However, if this peak is present, it is obscured by peak overlap.

Figure 8 shows the corresponding charge distributions and relative energy levels of full-sandwich ($m = n + 1$), half-sandwich ($m = n$), and inverted-sandwich ($m = n - 1$) neutral $Eu_n(COT)_m$ clusters. The lower panels of Figure 8 plot the corresponding PE spectra of $Eu_n(COT)_m^-$ and $Ba_n(COT)_m^-$. Additional discrete peaks appear in the 213 nm spectrum of larger clusters at higher binding energies (C1−C4); this feature is deconvoluted in some of the $Eu_n(COT)_m^-$ spectra by reference to the corresponding $Ba_n(COT)_m^-$ spectrum. Since photodetachment from Eu^{2+}/Ba^{2+} cations should require much higher energies,[48] all of these peaks are attributed to photodetachment from each COT^{2-} ligand.

The C1, C2, C3, and C4 peaks appear at the same energies in the $Eu_n(COT)_{n+1}$ and $Eu_n(COT)_n$ spectra. Notably, the higher excited states of C2, C3, and C4 in both spectra are located at energies similar to the C1, C2, and C3 peaks in the $Eu_n(COT)_{n-1}$ spectrum. This suggests that the electronic structure of the midsection is similar among the three $Eu_n(COT)_m$ cluster types, despite the charge differences of their terminal species.

As shown in Figure 8c, the peak M1 in the inverted-sandwich spectrum strongly depends on cluster size. Both the shifts and binding energies of peaks M and M1 are almost identical in the spectra of half-sandwich and inverted-sandwich clusters containing the same number of Eu atoms, i.e., $Eu_2(COT)_2$ and $Eu_2(COT)_1$, $Eu_3(COT)_3$ and $Eu_3(COT)_2$, and $Eu_4(COT)_4$ and $Eu_4(COT)_3$. In fact, the electron detachment channel in both cluster types can be assigned as $Eu^+ \rightarrow Eu^{2+}$. As discussed above, viewing from the terminal Eu^+ ion in $Eu_n(COT)_{n-1}^-$, incrementing the cluster size is equivalent to attaching an electric dipole, which stabilizes the detaching electron in Eu^+. The peak M1 in the $Eu_n(COT)_{n-1}^-$ spectrum is assignable to electron detachment from the anionic ground state (Figure 3i) to the first excited neutral state (state A in Figure 3h).

3.3. Formation Mechanism of $Eu_n(COT)_m$ Clusters. The $Eu_n(COT)_m$ chain is extended through a series of elementary processes that alternately stack the Eu atoms and COT ligands. Furthermore, the ionically bonded $Eu_n(COT)_m$ clusters presumably grow by successive electron transfer from Eu atoms to Eu−COT intermediates, or from Eu−COT intermediates to COT molecules, using the harpooning mechanism over long internuclear separations. As exemplified by the prototypal Li + F_2 "harpoon" reaction, the reaction path (entrance channel) is "downhill all the way"; i.e., no energy barrier intervenes during charge transfer (CT) with ion pair formation (e.g., $Li^+F_2^-$) at the early stage of the reaction.[35] The covalent and ionic potential energy surfaces are nearly degenerate, facilitating the transformation from covalent to ionic state, even over long distances (5−10 Å). In the harpoon mechanism, the energy difference (ΔE) between E_i and EA is related with a critical internuclear distance (R_c), at which CT reaction occurs from electron donor to acceptor, given by the following relation:[35]

$$R_c \cong \frac{e^2}{\Delta E} = \frac{14.35}{\Delta E\ (\text{eV})}\ (\text{Å}) \qquad (1)$$

Clearly, smaller ΔE allows a longer-range CT reaction. In other words, reactants with small E_i and high EA can interact through the CT reaction at large internuclear separations.

A full-sandwich configuration of $Eu_n(COT)_{n+1}$ extends its length by a series of further reactions. The four conceivable pathways are presented in Figure 9. In process I, a Eu atom attaches to one of the terminal COTs (n, $n + 1$). In process II, a resulting half-sandwich ($n + 1$, $n + 1$) extends its length via attachment of a COT ligand to its terminal Eu, forming an ($n + 1$, $n + 2$) full-sandwich cluster. Alternatively, if a Eu atom attaches to the terminal COT of ($n + 1$, $n + 1$) before the COT has terminated, an inverted-sandwich ($n + 2$, $n + 1$) should be formed (process III). Process IV yields an ($n + 2$, $n + 2$) half-sandwich by terminating either Eu end of ($n + 2$, $n + 1$) with COT. Note that full-sandwich and inverted-sandwich clusters

dx.doi.org/10.1021/jp5011007 | J. Phys. Chem. A XXXX, XXX, XXX−XXX

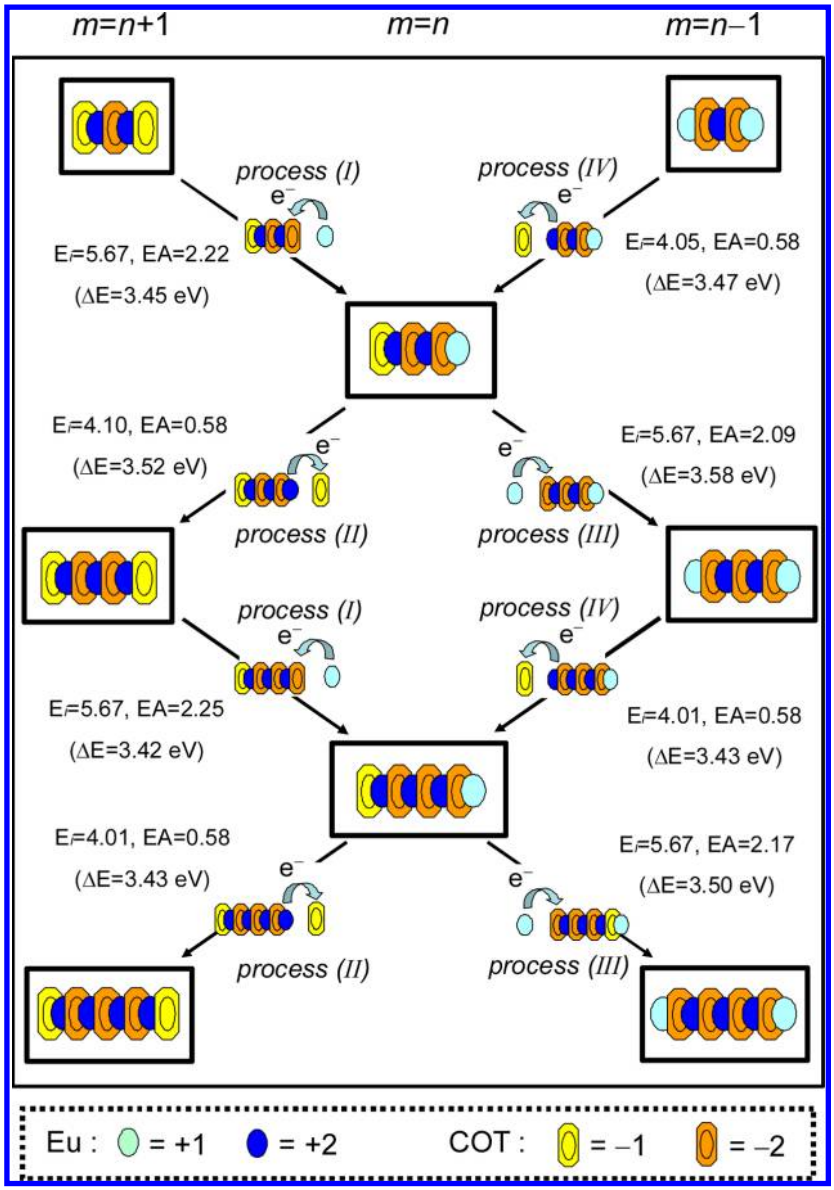

Figure 9. Energetics of Eu-COT growth for n = 2−5, obtained by photoionization and photoelectron spectroscopies. In every elementary step, the reaction preferentially proceeds between a low-E_i reactant and a high-EA reactant via the harpooning mechanism. The calculated endoergicity, ΔE, is ∼3.5 eV, and the apparent maximum internuclear separation, R_c, at which electron transfer can occur, is estimated as 4 Å. E_i and EA are specified in eV. Note that the charge distributions for the (3, 3) and (4, 4) neutrals correspond to those in the A state (diradical states) in Figure 3e.

have a reaction site at both ends, while half-sandwich clusters possess a single reaction site for process II or III. Therefore, the *effective* reaction probabilities of processes I and IV would be twice those of processes II and III. Such a kinetic effect (varying number of reaction sites) might explain the predominance of half-sandwich clusters in the mass spectra (see Figure 2) over full-sandwich and inverted-sandwich clusters.

To estimate the ΔE of processes I and II, we require the EA of full-sandwich $Eu_n(COT)_{n+1}$ and the E_i of half-sandwich $Eu_n(COT)_n$. Similarly, the ΔE of processes III and IV requires the EA of half-sandwich $Eu_n(COT)_n$ and the E_i of inverted-sandwich $Eu_n(COT)_{n-1}$. The E_i's and EAs of $Eu_n(COT)_m$ at each cluster size were obtained as described in sections 3.2.1 and 3.2.2. Given the E_i of Eu atoms (5.67 eV)[48] and the EAs of $Eu_n(COT)_{n+1}$ with n = 1−7 (∼2.2 eV), the ΔE of process I is calculated as 3.5 eV, yielding an R_c of 4.0 Å. Similarly, in process II, the E_i of $Eu_n(COT)_n$ is 4.3−4.0 eV (n = 2−4) and the EA of COT is 0.58 eV,[46,47] yielding ΔE = ∼3.4 eV and R_c = 3.9−4.2 Å (this analysis excludes the reaction $Eu_1(COT)_1$ + COT). The ΔE and R_c in processes III and IV are evaluated as ∼3.6 eV and 3.6−4.0 Å, respectively, since the EAs of half-sandwich $Eu_n(COT)_n$ clusters are ∼2.2 eV, while the E_i's of inverted-sandwich $Eu_n(COT)_{n-1}$ clusters (n > 2) are ∼4.2 eV. We emphasize that, in this analysis, all reactants are assumed as point masses with zero internal degrees of freedom.

Actual multiple-decker $Eu_n(COT)_m$ clusters possess highly anisotropic (rod-like) structures with tightly localized terminal reaction sites. Therefore, the R_c of each elementary process estimated here presumably corresponds to the average internuclear distance between a terminal end of the $Eu_n(COT)_m$ cluster and the Eu atom (or COT molecule) along the CT reaction coordinate. Consequently, every elementary reaction in the cluster growth process can exothermically occur at an apparent internuclear separation of

dx.doi.org/10.1021/jp5011007 | J. Phys. Chem. A XXXX, XXX, XXX−XXX

about 4 Å along the reaction coordinate, twice the equilibrium metal−ligand distance in the $Eu_n(COT)_m$ cluster (~2 Å).[36] Although its R_c is inferior to that of typical alkaline-halide systems (~10 Å),[35] the present system permits a relatively large reaction cross section σ_R (estimated as $\sigma_R \sim \pi R_c^2$). As discussed in section 3.2.2, furthermore, for $Eu_n(COT)_n$ neutrals (Figures 3e and 8b), the A state (diradical states) becomes more stable than the X state (closed-shell states) around n = 4, which preferably contributes to the CT reactions along the scheme in Figure 9. Hence, the above quantitative analysis of the experimental data rationalizes the successive CT reactions in the $Eu_n(COT)_m$ system that form super-multiple-decker sandwich clusters up to 12 nm in length.

4. CONCLUSIONS

Three different compositions of multiple-decker $Eu_n(COT)_m$ sandwich clusters, namely, full-sandwich $Eu_n(COT)_{n+1}$, half-sandwich $Eu_n(COT)_n$, and inverted-sandwich $Eu_n(COT)_{n-1}$, were exclusively produced in the gas phase by a laser-vaporization technique. The metal−ligand bonds in all clusters were highly ionic with commonly ordered charge distributions of Eu^{2+} and COT^{2-} ions, except at the termini, which were occupied with singly charged Eu^+ or COT^-. However, the ionization energies and electron affinities were almost independent of the cluster size in full- and inverted-sandwiches, but in half-sandwiches, the ionization energies were decreased and the electron affinities were increased asymptotically with the cluster size. These disparate size dependences can be understood by modeling an additional layer as a quadrupole or dipole in the electron detachment channel. A detaching electron from full- and inverted-sandwiches is stabilized by a quadrupole, whereas, for half sandwiches, it is stabilized by a dipole. Furthermore, in all cluster types, the terminal Eu^+ and COT^- reduces the E_i and raises the EA, respectively. Both phenomena promote harpoon-type formation of super-multiple-decker organometallic sandwich nanowires up to 12 nm in length. On the other hand, the internal electronic structure of the cluster types is very similar, on account of the strong polarization effect of the terminal Eu and Eu^+ in half- and inverted-sandwich clusters. The formal charge of polarized Eu and Eu^+ in the clusters is $Eu^{2+}COT^{2-}$ and $Eu^{2+}COT^-$, respectively. Thus, the internal electronic structure is similar among the three compositions because their charges are distributed in a full-sandwich configuration.

AUTHOR INFORMATION

Corresponding Author

*Phone: +81-45-566-1712. E-mail: nakajima@chem.keio.ac.jp.

Notes

The authors declare no competing financial interest.

ACKNOWLEDGMENTS

This work is partly supported by MEXT-Supported Program for the Strategic Research Foundation at Private Universities, 2009−2013. This work was also supported in part by the U.S. Department of Energy, Office of Basic Energy Sciences, Division of Chemical Sciences, under Contract W-31-109-ENG-38. N.H. is grateful to the Research Fellowship of JSPS for Young Scientists.

REFERENCES

(1) Kealy, T. J.; Pauson, P. L. A New Type of Organo-Iron Compound. *Nature* **1951**, *168*, 1039−1040.
(2) Powell, P. *Principles of Organometallic Chemistry*; Chapman and Hall: London, New York, 1988.
(3) Werner, H.; Salzer, A. Die Synthese Eines Ersten Doppel-Sandwich-Komplexes: Das Dinickeltricyclopentadienyl-Kation. *Synth. React. Inorg. Met.-Org. Chem.* **1972**, *2*, 239−248.
(4) Werner, H.; Salzer, A. Ein neuer Weg zu Tripeldeckersandwich-Verbindungen. *Angew. Chem.* **1972**, *84*, 949−950.
(5) Herrmann, W. A. *Synthetic Methods of Organometallic and Inorganic Chemistry*; Georg Thieme Verlag Stuttgart: New York, 1997.
(6) Hill, A. F. *Organotransition Metal Chemistry*; Wiley-RSC: Cambridge, 2002.
(7) Hoshino, K.; Kurikawa, T.; Takeda, H.; Nakajima, A.; Kaya, K. Structures and Ionization Energies of Sandwich Clusters (V_n(benzene)$_m$). *J. Phys. Chem.* **1995**, *99*, 3053−3055.
(8) van Heijnsbergen, D.; von Helden, G.; Meijer, G.; Maitre, P.; Duncan, M. A. Infrared spectra of gas-phase V^+-(benzene) and V^+-(benzene)$_2$ complexes. *J. Am. Chem. Soc.* **2002**, *124*, 1562−1563.
(9) Jaeger, T. D.; van Heijnsbergen, D.; Klippenstein, S. J.; von Helden, G.; Meijer, G.; Duncan, M. A. Vibrational Spectroscopy and Density Functional Theory of Transition-Metal Ion−Benzene and Dibenzene Complexes in the Gas Phase. *J. Am. Chem. Soc.* **2004**, *126*, 10981−10991.
(10) Weis, P.; Kemper, P. R.; Bowers, M. T. Structures and Energetics of $V_n(C_6H_6)_m^+$ Clusters: Evidence for a Quintuple-Decker Sandwich. *J. Phys. Chem. A* **1997**, *101*, 8207−8213.
(11) Rayane, D.; Allouche, A.-R.; Antoine, R.; Broyer, M.; Compagnon, I.; Dugourd, P. Electric dipole of metal−benzene sandwiches. *Chem. Phys. Lett.* **2003**, *375*, 506−510.
(12) Miyajima, K.; Muraoka, K.; Hashimoto, M.; Yasuike, T.; Yabushita, S.; Nakajima, A.; Kaya, K. The Quasi-Band Electronic Structure of V_n(Benzene)$_{n+1}$ Clusters. *J. Phys. Chem. A* **2002**, *106*, 10777−10781.
(13) Yasuike, T.; Yabushita, S. Ionization Energies and Bonding Scheme of Multiple-Decker Sandwich Clusters: $M_n(C_6H_6)_{n+1}$. *J. Phys. Chem. A* **1999**, *103*, 4533−4542.
(14) Goto, A.; Yabushita, S. Theoretical study on the spin states and intra-cluster spin relaxation of the one-dimensional metal-benzene sandwich clusters: $M_2(C_6H_6)_3$ (M═Sc,Ti,V). *Chem. Phys. Lett.* **2008**, *454*, 382−386.
(15) Miyajima, K.; Nakajima, A.; Yabushita, S.; Knickelbein, M. B.; Kaya, K. Ferromagnetism in One-Dimensional Vanadium-Benzene Sandwich Clusters. *J. Am. Chem. Soc.* **2004**, *126*, 13202−13203.
(16) Miyajima, K.; Knickelbein, M. B.; Nakajima, A. Stern-Gerlach Experiments of One-Dimensional Metal-Benzene Sandwich Clusters: $M_n(C_6H_6)_m$ (M = Al, Sc, Ti and V). *J. Am. Chem. Soc.* **2007**, *129*, 8473−8480.
(17) Kandalam, A. K.; Rao, B. K.; Jena, P.; Pandey, R. Geometry and electronic structure of $V_n(Bz)_m$ complexes. *J. Chem. Phys.* **2004**, *120*, 10414−10420.
(18) Wang, J.; Acioli, P. H.; Jellinek, J. Structure and Magnetism of V_nBz_{n+1} Sandwich Clusters. *J. Am. Chem. Soc.* **2005**, *127*, 2812−2813.
(19) Weng, H.; Taisuke Ozaki, T.; Terakura, K. Theoretical Analysis of Magnetic Coupling in Sandwich Clusters $V_n(C_6H_6)_{n+1}$. *J. Phys. Soc. Jpn.* **2008**, *77*, 014301-1−014301-9.
(20) Weng, H.; Taisuke Ozaki, T.; Terakura, K. Tailoring Magnetic Properties in Transition Metal−Benzene Sandwich Clusters: Ways to Design Molecular Magnets. *J. Phys. Soc. Jpn.* **2008**, *77*, 064301-1−064301-8.
(21) Weng, H.; Taisuke Ozaki, T.; Terakura, K. Revisiting magnetic coupling in transition-metal-benzene complexes with maximally localized Wannier functions. *Phys. Rev. B* **2009**, *79*, 235118-1−235118-8.
(22) Masubuchi, T.; Ohi, K.; Iwasa, T.; Nakajima, A. Experimental and theoretical studies on the electronic properties of vanadium-benzene sandwich cluster anions, V_nBz_{n+1}, (n = 1−5). *J. Chem. Phys.* **2012**, *137*, 224305-1−224305-9.

(23) Yasuike, T.; Nakajima, A.; Yabushita, S.; Kaya, K. Why do only vanadium atoms form multiple-decker sandwich clusters with benzene molecules ? *J. Phys. Chem. A* **1997**, *101*, 5360−5367.
(24) Cotton, S. *Lanthanide And Actinide Chemistry*; John Wiley & Sons, Ltd: West Sussex, 2006.
(25) Streitwieser, A., Jr.; Müller-Westerhoff, U. Bis-(cyclooctatetraenyl)uranium (uranocene). A new class of sandwich complexes that utilize atomic f orbitals. *J. Am. Chem. Soc.* **1968**, *90*, 7364−7364.
(26) Hayes, R. G.; Thomas, J. L. Synthesis of cyclooctatetraenyleuropium and cyclooctatetraenylytterbium. *J. Am. Chem. Soc.* **1969**, *91*, 6876−6876.
(27) Hodgson, K. O.; Mares, F.; Starks, D. F.; Streitwiser, A., Jr. Lanthanide(III) complexes with cyclooctatetraene dianion. Synthetic chemistry, characterization, and physical properties. *J. Am. Chem. Soc.* **1973**, *95*, 8650−8658.
(28) Liu, W.; Dolg, M.; Fulde, P. Low-lying electronic states of lanthanocenes and actinocenes $M(C_8H_8)_2$ (M═Nd, Tb, Yb, U). *J. Chem. Phys.* **1997**, *107*, 3584−3591.
(29) Liu, W.; Dolg, M.; Fulde, P. Calculated Properties of Lanthanocene Anions and the Unusual Electronic Structure of Their Neutral Counterparts. *Inorg. Chem.* **1998**, *37*, 1067−1072.
(30) Kurikawa, T.; Negishi, Y.; Hayakawa, F.; Nagao, S.; Miyajima, K.; Nakajima, A.; Kaya, K. Multiple-Decker Sandwich Complexes of Lanthanide - 1,3,5,7-Cyclooctatetraene $[Ln_n(C_8H_8)_m]$ (Ln = Ce, Nd, Eu, Ho, and Yb); Localized Ionic Bonding Structure. *J. Am. Chem. Soc.* **1998**, *120*, 11766−11772.
(31) Miyajima, K.; Kurikawa, T.; Hashimoto, M.; Nakajima, A.; Kaya, K. Charge Distributions in Multiple-Decker Sandwich Clusters of Lanthanide-Cyclooctatetraene: Application of Na Atom Doping. *Chem. Phys. Lett.* **1999**, *306*, 256−262.
(32) Miyajima, K.; Knickelbein, M. B.; Nakajima, A. Stern-Gerlach study of multidecker lanthanide-cyclooctatetraene sandwich clusters. *J. Phys. Chem. A* **2008**, *112*, 366−375.
(33) Scott, A. C.; Foster, N. R.; Grieves, G. A.; Duncan, M. A. Photodissociation of lanthanide metal cation complexes with cyclooctatetraene. *Int. J. Mass Spectrom.* **2007**, *263*, 171−178.
(34) Hosoya, N.; Takegami, R.; Suzumura, J.; Yada, K.; Koyasu, K.; Miyajima, K.; Mitsui, M.; Knickelbein, M. B.; Yabushita, S.; Nakajima, A. Lanthanide Organometallic Sandwich Nanowires: Formation Mechanism. *J. Phys. Chem. A* **2005**, *109*, 9−12.
(35) Levine, R. D.; Bernstein, R. B. *Molecular Reaction Dynamics and Chemical Reactivity*; Oxford University Press: New York, 1987.
(36) Takegami, R.; Hosoya, N.; Suzumura, J.; Yada, K.; Nakajima, A.; Yabushita, S. Ionization energies and electron distributions of one-end open sandwich clusters: Eu_n $(C_8H_8)_n$ (n = 1−4). *Chem. Phys. Lett.* **2005**, *403*, 169−174.
(37) Takegami, R.; Hosoya, N.; Suzumura, J.; Nakajima, A.; Yabushita, S. Geometric and Electronic Structures of Multiple-Decker One-End Open Sandwich Clusters: $Eu_n(C_8H_8)_n^-$ (n = 1−4). *J. Phys. Chem. A* **2005**, *109*, 2476−2486.
(38) Knickelbein, M. B. Electric dipole polarizabilities of Ni_{12-58}. *J. Chem. Phys.* **2001**, *115*, 5957−5964.
(39) Nakajima, A.; Kaya, K. A Novel Network Structure of Organometallic Clusters in Gas Phase. *J. Phys. Chem. A* **2000**, *104*, 176−191.
(40) Bucher, J. P.; Douglass, D. C.; Bloomfield, L. A. Pulsed supersonic source producing clusters with an adjustable vibrational temperature. *Rev. Sci. Instrum.* **1992**, *63*, 5667−5670.
(41) Hotop, H.; Lineberger, W. C. Binding Energies in Atomic Negative Ions. *J. Phys. Chem. Ref. Data* **1975**, *4*, 539−576.
(42) Esaulov, V. A. Electron detachment from atomic negative ions. *Ann. Phys. Fr.* **1986**, *11*, 493−592.
(43) Miyajima, K.; Knickelbein, M. B.; Nakajima, A. Stern-Gerlach studies of organometallic sandwich clusters. *Eur. Phys. J. D* **2005**, *34*, 177−182.
(44) Wenthold, P. G.; Hrovat, D. A.; Borden, W. T.; Lineberger, W. C. Transition-State Spectroscopy of Cyclooctatetraene. *Science* **1996**, *272*, 1456−1459.
(45) Corderman, R. R.; Engelking, P. C.; Lineberger, W. C. Laser photoelectron spectrometry of Co^- and Ni^-. *J. Chem. Phys.* **1979**, *70*, 4474−4480.
(46) Wentworth, W. E.; Ristau, W. Thermal electron attachment involving a change in molecular geometry. *J. Phys. Chem.* **1969**, *73*, 2126−2133.
(47) Denault, J. W.; Chen, G. D.; Cooks, R. G. Electron affinity of 1,3,5,7-cyclooctatetraene determined by the kinetic method. *J. Am. Soc. Mass Spectrom.* **1998**, *9*, 1141−1145.
(48) Lide, D. R. *CRC Handbook of Chemistry and Physics*, 84th ed.; CRC Press: Boca Raton, FL, 2003.

dx.doi.org/10.1021/jp5011007 | *J. Phys. Chem. A* XXXX, XXX, XXX−XXX